JACS
JOURNAL OF THE AMERICAN CHEMICAL SOCIETY
Article
pubs.acs.org/JACS

# Solution-Phase Mechanistic Study and Solid-State Structure of a Tris(bipyridinium radical cation) Inclusion Complex

Albert C. Fahrenbach,[†,⊥] Jonathan C. Barnes,[†,⊥] Don Antoine Lanfranchi,[‡] Hao Li,[†] Ali Coskun,[†,⊥] Jeremiah J. Gassensmith,[†] Zhichang Liu,[†] Diego Benítez,[§] Ali Trabolsi,[†,∥] William A. Goddard III,[§,⊥] Mourad Elhabiri,*[,‡] and J. Fraser Stoddart*[,†,⊥]

[†]Department of Chemistry, Northwestern University, 2145 Sheridan Road, Evanston, Illinois 60208, United States

[‡]Laboratoire de Chimie Bioorganique et Médicinale, UMR 7509 CNRS-UdS, ECPM, Université de Strasbourg, 25 rue Becquerel, 67200 Strasbourg, France

[§]Materials and Process Simulation Center, California Institute of Technology, Pasadena, California 91125, United States

[∥]Center for Science and Engineering, New York University Abu Dhabi, Abu Dhabi, United Arab Emirates

[⊥]NanoCentury KAIST Institute and Graduate School of EEWS (WCU), Korea Advanced Institute of Science and Technology (KAIST), 373-1 Guseong Dong, Yuseong Gu, Daejeon 305-701, Republic of Korea

Supporting Information

**ABSTRACT:** The ability of the diradical dicationic cyclobis(paraquat-*p*-phenylene) ($CBPQT^{2(\bullet+)}$) ring to form inclusion complexes with 1,1′-dialkyl-4,4′-bipyridinium radical cationic ($BIPY^{\bullet+}$) guests has been investigated mechanistically and quantitatively. Two $BIPY^{\bullet+}$ radical cations, methyl viologen ($MV^{\bullet+}$) and a dibutynyl derivative ($V^{\bullet+}$), were investigated as guests for the $CBPQT^{2(\bullet+)}$ ring. Both guests form trisradical complexes, namely, $CBPQT^{2(\bullet+)}\subset MV^{\bullet+}$ and $CBPQT^{2(\bullet+)}\subset V^{\bullet+}$, respectively. The structural details of the $CBPQT^{2(\bullet+)}\subset MV^{\bullet+}$ complex, which were ascertained by single-crystal X-ray crystallography, reveal that $MV^{\bullet+}$ is located inside the cavity of the ring in a centrosymmetric fashion: the 1:1 complexes pack in continuous radical cation stacks. A similar solid-state packing was observed in the case of $CBPQT^{2(\bullet+)}$ by itself. Quantum mechanical calculations agree well with the superstructure revealed by X-ray crystallography for $CBPQT^{2(\bullet+)}\subset MV^{\bullet+}$ and further suggest an electronic asymmetry in the SOMO caused by radical-pairing interactions. The electronic asymmetry is maintained in solution. The thermodynamic stability of the $CBPQT^{2(\bullet+)}\subset MV^{\bullet+}$ complex was probed by both isothermal titration calorimetry (ITC) and UV/vis spectroscopy, leading to binding constants of $(5.0 \pm 0.6) \times 10^4$ $M^{-1}$ and $(7.9 \pm 5.5) \times 10^4$ $M^{-1}$, respectively. The kinetics of association and dissociation were determined by stopped-flow spectroscopy, yielding a $k_f$ and $k_b$ of $(2.1 \pm 0.3) \times 10^6$ $M^{-1}$ $s^{-1}$ and $250 \pm 50$ $s^{-1}$, respectively. The electrochemical mechanistic details were studied by variable scan rate cyclic voltammetry (CV), and the experimental data were compared digitally with simulated data, modeled on the proposed mechanism using the thermodynamic and kinetic parameters obtained from ITC, UV/vis, and stopped-flow spectroscopy. In particular, the electrochemical mechanism of association/dissociation involves a bisradical tetracationic intermediate $CBPQT^{(2+)(\bullet+)}\subset V^{\bullet+}$ inclusion complex; in the case of the $V^{\bullet+}$ guest, the rate of disassociation ($k_b = 10 \pm 2$ $s^{-1}$) was slow enough that it could be detected and quantified by variable scan rate CV. All the experimental observations lead to the speculation that the $CBPQT^{(2+)(\bullet+)}$ ring of the bisradical tetracation complex might possess the unique property of being able to recognize both $BIPY^{\bullet+}$ radical cation and π-electron-rich guests simultaneously. The findings reported herein lay the foundation for future studies where this radical−radical recognition motif is harnessed particularly in the context of mechanically interlocked molecules and increases our fundamental understanding of $BIPY^{\bullet+}$ radical−radical interactions in solution as well as in the solid-state.

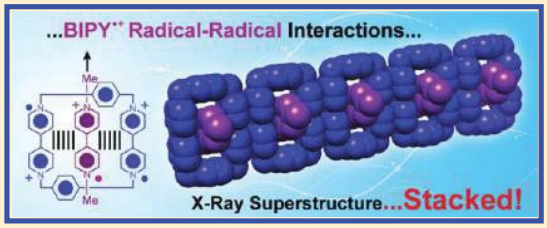


## INTRODUCTION

Noncovalent donor−acceptor charge-transfer (CT) interactions, which occur[1] between π-electron-poor 1,1′-dialkyl-4,4′-bipyridinium ($BIPY^{2+}$) dications and a range of neutral π-electron-rich compounds have been known[2] since at least the 1960s. Since these times, the blossoming of the systematic investigation of noncovalent bonding interactions in general that followed hard on the heels of the discovery[3] of the crown ethers[4] by Pedersen[5] led directly to the development of host−guest chemistry[6] by Cram[7] and the ushering in of chemistry beyond the molecule, later to become known as supramolecular chemistry[8] at the suggestion of Lehn.[9] Both host−guest and supramolecular chemistry have evolved to embrace inclusion complexes of many different types, including those of a donor−acceptor nature where $BIPY^{2+}$ units fulfill the role of guests[10] in some cases and of components of hosts[11] in others. The large collection[12] of stable donor−acceptor complexes involving

Received: September 23, 2011
Published: December 9, 2011

ACS Publications © 2011 American Chemical Society

dx.doi.org/10.1021/ja2089603 | J. Am. Chem.Soc. 2012, 134, 3061−3072

**Scheme 1. Conceptual Portrayals of the Donor–Acceptor Interactions That Ensue between π-Electron-Poor $BIPY^{2+}$ (Acceptor) Units in Their Fully Oxidized States and π-Electron-Rich (Donor) Units and, upon Reduction to Their $BIPY^{\bullet+}$ Radical Cations, the Self-Loving, Radical–Radical Interactions That Exist between the Radical Cations[a]**

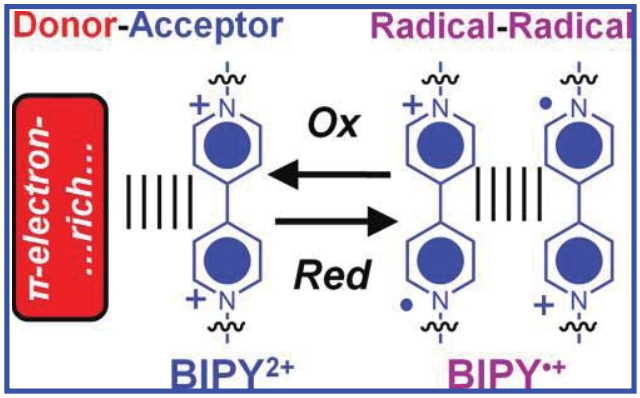


[a]Although many examples of donor–acceptor recognition motifs have been described in the literature, relatively few radical–radical inclusion complexes have been reported in communications and papers.

$BIPY^{2+}$ units as π-electron-poor acceptors alongside a suite of π-electron-rich donors has resulted in the use of donor–acceptor interactions to template the formation of the mechanical bond,[13] paving the way for the development[14] of mechanically interlocked molecules (MIMs) such as catenanes[15] and rotaxanes.[16] The introduction of bistability into these MIMs has transformed them from being intellectual curiosities into functioning molecular switches, which have been incorporated into integrated systems as disparate as molecular electronic devices[17] (MEDs) in addressable memories[18] based on crossbar architectures, artificial molecular muscles[19] as examples of nanoelectromechanical systems (NEMS), and mechanized mesoporous silica nanoparticles (MSNPs) for drug delivery.[20]

The radical chemistry of compounds containing $BIPY^{2+}$ units has been well documented[21] in the scientific literature since the 1930s. They have been referred to commonly[21b] as viologen salts having acquired this name because, upon their reduction to $BIPY^{\bullet+}$ radical cations in aqueous solutions, they acquire a vibrant purple color, which was ascribed in 1964 by Kosower[22] to the coming together of two radical cations to produce a $[(BIPY^{\bullet+})_2]$ dimer. On dilution, the purple color recedes and the aqueous solution becomes blue on account of the dissociation of the of the $[(BIPY^{\bullet+})_2]$ dimer into the $BIPY^{\bullet+}$ radical cation monomer.

Despite the fact that $BIPY^{\bullet+}$ radical cations have been known[22,23] for over 40 years to undergo dimerization, sometimes referred to as pimerization,[24] under appropriate conditions, it is not so long ago that researchers began to synthesize host–guest systems that take advantage of the tendency for $BIPY^{\bullet+}$ radical cations to dimerize. In many ways, their self-recognizing radical–radical interactions serve (Scheme 1) to supplement the classical donor–acceptor interactions that occur in the fully oxidized form, that is, the $BIPY^{2+}$ dication, with π-electron-rich donors. Kimoon Kim,[25] for example, has demonstrated that $BIPY^{\bullet+}$ radical cation dimers can be included inside the cavity of cucurbit[8]uril. On the other hand, we have discovered[26] very recently the ability of the cyclobis(paraquat-*p*-phenylene) ($CBPQT^{4+}$) ring, which is composed of two $BIPY^{2+}$ units held rigidly in place approximately 7 Å apart, when reduced to the diradical dication $CBPQT^{2(\bullet+)}$, to form stable trisradical tricationic inclusion complexes with appropriate guests containing $BIPY^{\bullet+}$ radical cationic centers on account of favorable radical–radical interactions. Moreover, we have demonstrated[26b] that these radically stabilized inclusion complexes can act as an efficient means of templating the formation of mechanical bonds in the synthesis of a [2]rotaxane, employing[13,27] a threading-followed-by-stoppering approach.

In this paper, we describe the various methods that we have employed to probe the mechanism of formation of a trisradical tricationic inclusion complex involving the $CBPQT^{2(\bullet+)}$ diradical dication, which encircles spontaneously $BIPY^{\bullet+}$-containing guests, namely, methyl viologen ($MV^{\bullet+}$) and also a butynyl derivative ($V^{\bullet+}$), provided they are in their radical cationic redox states. We reveal that a bisradical tetracationic inclusion complex plays an important role as an intermediate in the redox-induced switching processes. Structural, thermodynamic, and kinetic parameters have all been elucidated using (i) single-crystal X-ray crystallography, (ii) quantum mechanical calculations, (iii) isothermal titration calorimetry (ITC) supported by UV/vis spectroscopy, and (iv) stopped-flow UV/vis spectroscopy, complemented by (v) variable scan rate cyclic voltammetry (CV) in conjunction with (vi) digital simulations based on the proposed mechanism for the complexation.

## RESULTS AND DISCUSSION

Following a three-electron reduction, one going into each of the $BIPY^{2+}$ units of the $CBPQT^{4+}$ ring and one electron entering the $BIPY^{2+}$ unit of the $MV^{2+}$ guest, a stable thermodynamic state arises whereby the $CBPQT^{2(\bullet+)}$ ring encircles the $MV^{\bullet+}$ radical cation. The structural formulas and graphical representations of the [2]pseudorotaxane $CBPQT^{2(\bullet+)}\subset MV^{\bullet+}$, along with the simplified schematic of the redox-induced complexation processes, are illustrated in Scheme 2. Previously, we have shown[26a] both experimentally and theoretically in solution that, because only two of the $BIPY^{\bullet+}$ radical cations of the complex are spin-paired at any

**Scheme 2. Simplified Schematic Representation Using Structural Formulas of the Redox-Induced Formation of the Trisradical Cationic Inclusion Complex $CBPQT^{2(\bullet+)}\subset MV^{\bullet+}$ and Its Graphical Representation[a]**

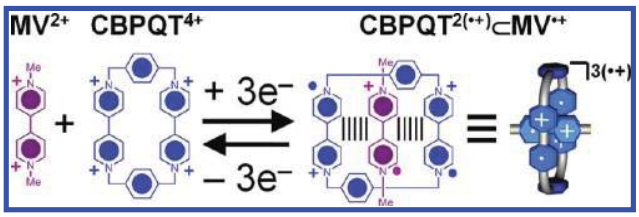


[a]Upon a three-electron reduction of an equimolar mixture of $CBPQT^{4+}$ and $MV^{2+}$, the $MV^{\bullet+}$ radical cation is included spontaneously inside the cavity of the $CBPQT^{2(\bullet+)}$ diradical dication ring as a result of favorable radical–radical interactions occurring between the three $BIPY^{\bullet+}$ radical cations. Reoxidation of the tricationic complex results in the regeneration of the initial uncomplexed $CBPQT^{4+}$ host and $MV^{2+}$ guest. For a more complete mechanistic description, see Figure 7 and the Supporting Information.


dx.doi.org/10.1021/ja2089603 | J. Am. Chem.Soc. 2012, 134, 3061–3072

given time, the third unpaired $BIPY^{\bullet+}$ radical cation of the complex is not as strongly engaged in radical–radical interactions. This fact has important repercussions for the redox-induced mechanism of switching, which will be discussed in detail later on in this paper. Reoxidation of the complex results in its dissociation into its constituent components. Overall, the complexation and decomplexation processes are reversible.

**X-ray Crystallography.** Single crystals of the $CBPQT^{2(\bullet+)}\subset MV^{\bullet+}$ complex were grown from MeCN using slow vapor diffusion of $iPr_2O$ inside a glovebox at room temperature. Zinc dust was used to bring about[28] the reduction of $CBPQT^{4+}$ and $MV^{2+}$ to their respective radical cationic forms. (For a general procedure on the use of zinc dust as a reducing agent, see the Experimental Section). The solid-state structure,[29] as determined by X-ray crystallography,[30] demonstrates (Figure 1) the formation of the trisradical tricationic complex. The inclusion complex was observed to be associated with three $PF_6^-$ counterions in the solid state, supporting the hypothesis that each of the $BIPY^{2+}$ units indeed has been reduced to their radical cationic form, $BIPY^{\bullet+}$. The $MV^{\bullet+}$ radical cation is situated inside the cavity of the $CBPQT^{2(\bullet+)}$ ring in a centrosymmetric fashion, with 3.22 Å centroid-to-centroid separation from each of the $BIPY^{\bullet+}$ radical cation subunits of the cyclophane. The axis defined by the central aryl–aryl C–C bond in the $MV^{\bullet+}$ radical cation subtends an angle of 14° (Figure 1b) with the axis orthogonal to the plane defined by the four N atoms of the ring. We surmise that this deviation from orthogonality maximizes[31] the amount of $\pi$-overlap between $MV^{\bullet+}$ and $CBPQT^{2(\bullet+)}$. This deviation from orthogonality observed in the solid state for the $CBPQT^{2(\bullet+)}\subset MV^{\bullet+}$ complex is in good agreement (*vide infra*) with that predicted from theoretical calculations. Virtually no torsional twisting of any of the three $BIPY^{\bullet+}$ units of the complex about their 4,4′-C–C bond is apparent, a phenomenon that is not observed for the $CBPQT^{4+}$ ring in its fully oxidized form. This almost complete lack of torsional twists is consistent, however, with the solid-state structure of the $MV^{\bullet+}$ radical cation reported[32] previously. The extended superstructure reveals (Figure 1c) a continuous $BIPY^{\bullet+}$ radical cation $\pi$-stack, with adjacent complexes aligned in register. A centroid-to-centroid separation of 3.28 Å characterizes the distance between the $BIPY^{\bullet+}$ radical cation subunits of the $CBPQT^{2(\bullet+)}$ of adjacent complexes. The $PF_6^-$ counterions are observed to occupy (Figure 1d) the space between adjacent stacks. In particular, close contact (~2.6 Å) of the fluorines with the hydrogen atoms of the methylene groups and those of the $\alpha$ and $\beta$ carbons of the $CBPQT^{2(\bullet+)}$ ring are observed. In all, this type of continuous radical cation stack is similar to that reported by Kochi[32] in 1990 for the $MV^{\bullet+}$ radical cation in the solid state.

We have also investigated the crystal growth of the $CBPQT^{2(\bullet+)}$ diradical dication alone in solution. Crystals were obtained from slow vapor diffusion of $iPr_2O$ into a solution of the diradical dication in MeCN all inside of a glovebox. Remarkably, long, dark, opaque needle-like crystals up to three centimeters in length were observed after less than a week of crystal growth. Single-crystal X-ray analyses[30] revealed[29] (Figure 2) that $CBPQT^{2(\bullet+)}$ crystallizes with two $PF_6^-$ counterions, confirming its diradical dicationic nature. Once again, virtually no torsional twisting was observed in the $BIPY^{\bullet+}$ units of the $CBPQT^{2(\bullet+)}$ ring, an observation that is consistent with that already observed for the trisradical

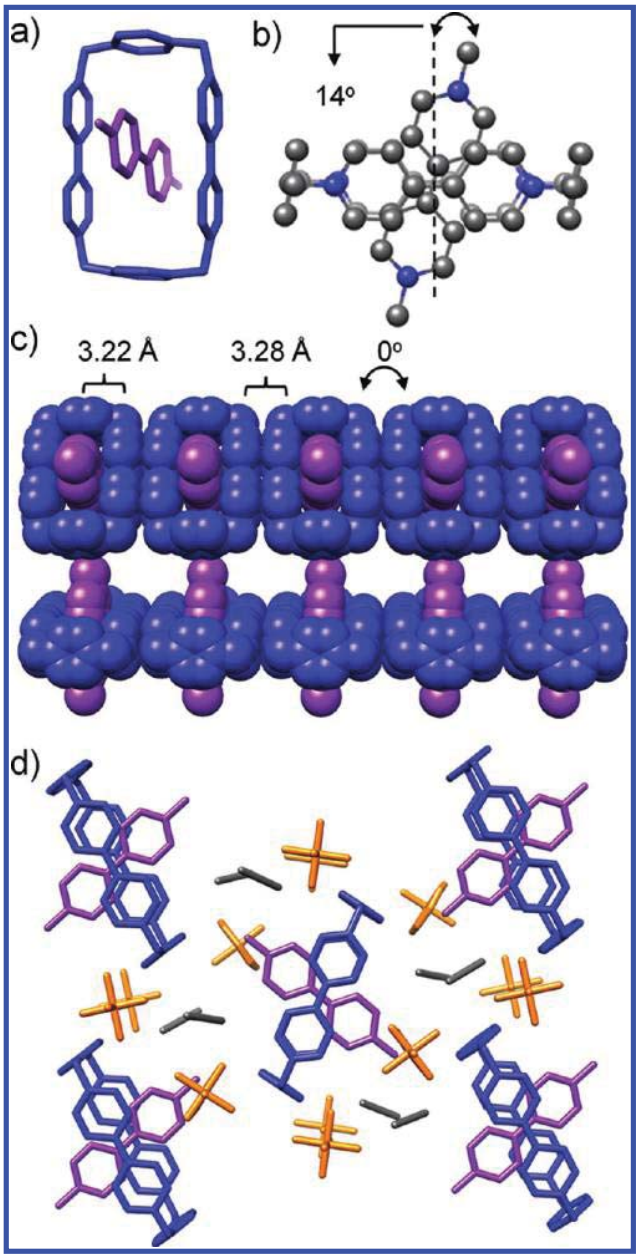


**Figure 1.** Solid-state superstructures of the trisradical cation $CBPQT^{2(\bullet+)}\subset MV^{\bullet+}$ inclusion complex obtained by single-crystal X-ray crystallography. (a) Wireframe representation of the $CBPQT^{2(\bullet+)}\subset MV^{\bullet+}$ inclusion complex. (b) Ball-and-stick representation of the $CBPQT^{2(\bullet+)}\subset MV^{\bullet+}$ inclusion complex from a side-on perspective, illustrating the angle of offset from orthogonality of the $MV^{\bullet+}$ occupying the cavity of $CBPQT^{2(\bullet+)}$. (c) Space-filling representation along the *a*-axis of the long-range packing order of the trisradical tricationic $CBPQT^{2(\bullet+)}\subset MV^{\bullet+}$ inclusion complex, which forms a continuous radical–radical $\pi$-stack. The $PF_6^-$ counterions have been omitted for clarity. (d) Side-on view of the unit cell of the $CBPQT^{2(\bullet+)}\subset MV^{\bullet+}$ inclusion complex determined by X-ray crystallography revealing the superstructure and relative positioning of the $PF_6^-$ counterions and MeCN solvent molecules.

complex. The centroid-to-centroid transannular distance spanning the gap between the planes of the two $BIPY^{\bullet+}$ units of the ring is 6.92 Å, a remarkably longer distance compared with that (6.43 Å) present in the trisradical complex.


dx.doi.org/10.1021/ja2089603 | *J. Am. Chem.Soc.* 2012, 134, 3061–3072

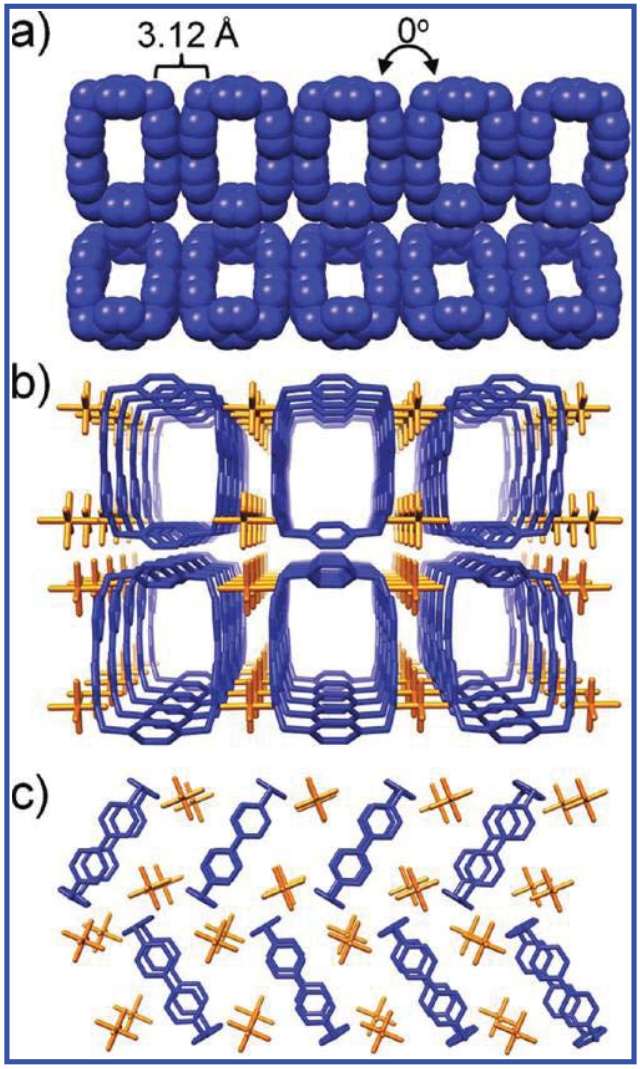


**Figure 2.** Solid-state superstructure of the diradical dication $CBPQT^{2(\bullet+)}$ ring obtained by single-crystal X-ray crystallography. (a) In common with the trisradical $CBPQT^{2(\bullet+)}\subset MV^{\bullet+}$ inclusion complex, the $CBPQT^{2(\bullet+)}$ solid-state superstructure reveals a stack of $CBPQT^{2(\bullet+)}$ rings along the *a* crystallographic axis maintained by interactions between its $BIPY^{\bullet+}$ constituent subunits. The counterions, $PF_6^-$, have been omitted for clarity. (b) A wireframe representation of the solid-state superstructure of $CBPQT^{2(\bullet+)}$, depicting the porous channels formed by the diradical dicationic ring's unoccupied interiors. (c) Side-on view of the X-ray structure of the $CBPQT^{2(\bullet+)}$ revealing the superstructure and relative positioning of the $PF_6^-$ counterions.

The centroid-to-centroid transannular separation between the phenylene units, which was observed in the solid-state structure of the $CBPQT^{2(\bullet+)}$ ring, is 10.2 Å and may be contrasted with the analogous distance of 10.3 Å for the trisradical complex. These observations indicate that the $CBPQT^{2(\bullet+)}$ ring is able to expand in size in one direction while contracting in the other in order to accommodate the $MV^{\bullet+}$ guest in such a way that the bowing of the $BIPY^{\bullet+}$ units of the ring is reduced. The decreased degree of bowing of the $BIPY^{\bullet+}$ units brought about by the inclusion of $MV^{\bullet+}$ in the $CBPQT^{2(\bullet+)}$ ring serves to increase the distance between the phenylene units of the ring in the complex. Reminiscent of the way the trisradical complex packs in the solid state, the superstructure reveals a continuous stack of $CBPQT^{2(\bullet+)}$ rings. A centroid-to-centroid separation between the $BIPY^{\bullet+}$ units of adjacent $CBPQT^{2(\bullet+)}$ rings of 3.12 Å is observed along with a packing structure that is aligned in register, that is, no angle of offset between adjacently stacked rings is observed. The cavities of the rings arrange themselves in such a way as to form (Figure 2b) continuous porous channels that run the whole length of the crystal, with the $PF_6^-$ counterions occupying the spaces between the rings. In a fashion similar to that of the trisradical complex, close contact (~2.6 Å) of the fluorine atoms with the *α*, *β*, and methylene protons of the $CBPQT^{2(\bullet+)}$ ring is observed (Figure 2c). Overall, the superstructure is consistent with our understanding of the nature of $BIPY^{\bullet+}$ radical−radical interactions, which serve to "stitch" the $CBPQT^{2(\bullet+)}$ rings together into stacks.

**Quantum Mechanical Calculations.** In order to gain a better understanding of the nature of the binding in $CBPQT^{2(\bullet+)}\subset MV^{\bullet+}$, we have previously used[26a] density functional theory[33] of the M06 flavor[34] to provide a quantum mechanical description of the binding in the superstructure. The superstructure for $[CBPQT^{2(\bullet+)}\subset MV^{\bullet+}][3PF_6^-]$ was minimized at the M06/6-31G** level, as depicted in Figure 3a. The calculated superstructure (Figure 3a) agrees well with that determined experimentally from X-ray crystallography, namely, that $MV^{\bullet+}$ resides inside the cavity of the $CBPQT^{2(\bullet+)}$ ring at an angle offset to the axis perpendicular to the plane defined by the four nitrogen atoms of the ring. Natural population analysis[35] of the inclusion complex shows that the charges on the $CBPQT^{2(\bullet+)}$ and $MV^{\bullet+}$ fragments are +1.71 and +1.18, respectively, which suggests some degree of charge transfer from the guest to the host. The asymmetry of the complex is also corroborated by the singly occupied molecular orbital (SOMO) being preferentially distributed (Figure 3b) over one of the two $BIPY^{\bullet+}$ units of the $CBPQT^{2(\bullet+)}$ ring. This electronic asymmetry in the SOMO supports our hypothesis (*vide infra*) that, as a consequence of radical pairing, one $BIPY^{\bullet+}$ unit of the $CBPQT^{2(\bullet+)}$ ring is not interacting as strongly with the $MV^{\bullet+}$ guest. As a result, this weaker interaction of one $BIPY^{\bullet+}$ unit of the $CBPQT^{2(\bullet+)}$ ring leads to a bisradical tetracationic $CBPQT^{(2+)(\bullet+)}\subset MV^{\bullet+}$ intermediate in the electrochemical mechanism of formation. In addition, the $MV^{\bullet+}$ guest in the

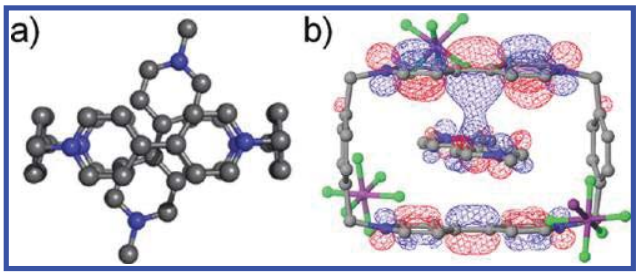


**Figure 3.** Results from quantum mechanical calculations of the trisradical $CBPQT^{2(\bullet+)}\subset MV^{\bullet+}$ complex minimized at the M06/6-31G** level of DFT. (a) Calculated structure (side view) of the trisradical $CBPQT^{2(\bullet+)}\subset MV^{\bullet+}$ complex with the $PF_6^-$ counterions omitted for clarity. (b) Character of the singly occupied molecular orbital (SOMO), where positive and negative phases are shaded blue and red. The SOMO is asymmetrically distributed toward the top $BIPY^{\bullet+}$ radical cation subunit of the $CBPQT^{2(\bullet+)}$ ring component, a distribution of which is likely exaggerated by the asymmetry in the locations of the $PF_6^-$ counterions. In the ball-and-stick representation of the framework, C is black, N is blue, F is green, and P is purple.


dx.doi.org/10.1021/ja2089603 | *J. Am. Chem.Soc.* 2012, 134, 3061−3072

calculated structure is located ~0.14 Å closer to one of the $BIPY^{\bullet+}$ units in the $CBPQT^{2(\bullet+)}$ ring. Additional polarization affects brought about by the asymmetric positioning of the three $PF_6^-$ counterions may act to further exaggerate this distribution of electron density in the SOMO as well as influence the location of the guest within the host. The fact that the crystal structure reveals that the $MV^{\bullet+}$ guest resides equidistant from either side of the $BIPY^{\bullet+}$ units of the $CBPQT^{2(\bullet+)}$ ring is most likely a consequence of the continuous radical−radical packing superstructure, with the $PF_6^-$ counterions symmetrically placed on either side of each complex, which probably serves to "wash-out" this asymmetry in the solid state. We hypothesize that the electronic asymmetry predicted by theory continues to live-on in the solution phase, where no such stacking of complexes is occurring.

**Isothermal Titration Calorimetry.** Thermodynamic parameters governing the stability of the trisradical complex in solution have been obtained by performing ITC experiments at room temperature in MeCN under the inert conditions provided by a glovebox. Solutions of $CBPQT^{2(\bullet+)}$ and $MV^{\bullet+}$ were prepared individually using zinc dust as the reducing agent. The results (Figure 4) confirm the 1:1 stoichiometry of the complex and reveal an association constant ($K_a$) of $(5.0 \pm 0.6) \times 10^4$ $M^{-1}$. As expected, the binding is enthalpically driven by a $\Delta H$ value of $-15.2 \pm 0.5$ kcal $mol^{-1}$ for an entropic cost of $-29.3 \pm 1.6$ cal $mol^{-1}$ $K^{-1}$ in $\Delta S$. The free energy of formation $\Delta G$ at 298 K is $-6.41 \pm 0.07$ kcal $mol^{-1}$. By comparison with the free energies of formation determined[36] under identical conditions for classical donor−acceptor complexes involving the fully oxidized tetracationic $CBPQT^{4+}$ ring and the $\pi$-electron-rich guests, 1,5-bis[2-(2-hydroxyethoxy)ethoxy]-naphthalene (BHEEN) ($\Delta G = -6.26 \pm 0.04$ kcal $mol^{-1}$) and 2-[2-[[2-[4-[[2-(2-hydroxyethoxy)ethoxy]methyl]-1,3-dithiol-2-ylidene]-1,3-dithiol-4-yl]methoxy]ethoxy]ethanol (a bis(di-(ethylene glycol))tetrathiafulvalene derivative) ($\Delta G = -7.66 \pm 0.07$ kcal $mol^{-1}$), one finds that the binding energy is on a par with these complexes. In these donor−acceptor complexes, a significant amount of the binding energy comes[37] from [C−H···O] interactions involving particularly the terminal oxygen atoms of the oligo(ethylene glycol) chains to the hydrogen atoms of the $\alpha$ carbons in the ring. The additional affinity gained from these [C−H···O] interactions is lost when the glycol chains are not present. It is worth noting that, in the case of the trisradical complex in MeCN, [C−H···O] interactions are not necessary in order to achieve binding constants of similar orders of magnitude. The binding affinities for the $CBPQT^{4+}$ ring, as measured previously[36] by ITC in MeCN at 298 K, for tetrathiafulvalene and 1,5-dihydroxynaphthalene, both of which lack oligo(ethylene glycol) chains, were determined to be $(6.9 \pm 0.18) \times 10^3$ $M^{-1}$ and $440 \pm 130$ $M^{-1}$, respectively.

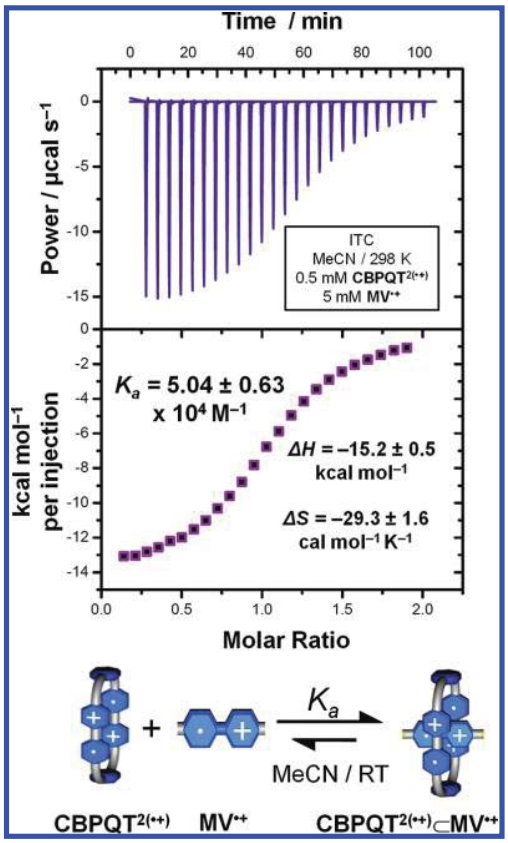


**Figure 4.** The isothermal titration calorimetry (ITC) traces obtained when measuring the thermodynamic parameters ($K_a$, $\Delta H$, $\Delta S$) governing the formation of the trisradical $CBPQT^{2(\bullet+)}\subset MV^{\bullet+}$ inclusion complex. All the ITC experiments were performed in MeCN at 298 K. The values for $K_a$, $\Delta H$ and $\Delta S$ reported above are averages over four runs, and the errors are the associated standard deviations from these four runs.

**UV/Vis and Stopped-Flow Spectroscopy.** The absorption spectra of the radical cation $MV^{\bullet+}$ and of the diradical dication $CBPQT^{2(\bullet+)}$ were first of all recorded alone in MeCN at concentrations in the range of $\sim 5 \times 10^{-5}$ to $10^{-4}$ M in order to verify the absence of intermolecular radical−radical interactions[38] between like species under the experimental conditions employed. The absorption spectra of $MV^{\bullet+}$ and of $CBPQT^{2(\bullet+)}$ are both characterized (Figure 5a) by two sets of finely structured absorptions (vibronic coupling) centered on 390 and 600 nm, respectively. No absorption was observed in the near-IR region, an observation that confirms the absence[39] of intermolecular radical−radical interactions, namely, $BIPY^{\bullet+}$ dimerization, in MeCN.

The electronic spectrum of $CBPQT^{2(\bullet+)}$ was compared (Supporting Information) to the sum of the electronic spectra of 2 equiv. of $MV^{\bullet+}$ in order to further investigate the ability of the two $BIPY^{\bullet+}$ units in $CBPQT^{2(\bullet+)}$ to interact with each other in a noncovalent bonding fashion. The larger extinction coefficients (Supporting Information) of the $CBPQT^{2(\bullet+)}$ diradical dication, compared to the sum of two $MV^{\bullet+}$ radical cations, suggest an intramolecular dipole−dipole interaction in the ground state between the $CBPQT^{2(\bullet+)}$ ring's two $BIPY^{\bullet+}$ radical cationic units. This observation is in good agreement[40] with EPR results obtained previously, data from which support the hypothesis of intramolecular dipole−dipole interactions.

The strength of the association between $CBPQT^{2(\bullet+)}$ and the $MV^{\bullet+}$ was then probed (Supporting Information) in MeCN using UV/vis absorption spectrophotometry, allowing us to assess the spectroscopic and thermodynamic parameters associated with the formation of the $CBPQT^{2(\bullet+)}\subset MV^{\bullet+}$ trisradical trication inclusion complex. The recognition of $MV^{\bullet+}$ by $CBPQT^{2(\bullet+)}$ occurs (Figure 5a) with a significant broadening of the absorption band centered around 604 nm, resulting effectively in the concomitant observation of a new band appearing at 550 nm, as well as the emergence[41] of an intense absorption band straddling[26a] the near-IR region.


dx.doi.org/10.1021/ja2089603 | J. Am. Chem.Soc. 2012, 134, 3061−3072

**Table 1. Thermodynamic Parameters Associated with the Formation of the Trisradical Inclusion Complex between the Diradical Dication $CBPQT^{2(\bullet+)}$ Ring and the Radical Cation $MV^{\bullet+}$[a]**

| | $K_a$, $10^4$ $M^{-1}$ | $\Delta G$, kcal $mol^{-1}$ | $\Delta H$, kcal $mol^{-1}$ | $\Delta S$, cal $mol^{-1}$ $K^{-1}$ |
|---|---|---|---|---|
| $CBPQT^{2(\bullet+)}\subset MV^{\bullet+}$ | 5.04 ± 0.63[b] | −6.41 ± 0.07[b] | −15.2 ± 0.5[b] | −29.3 ± 1.6[b] |
| | 7.9 ± 5.5[c] | −6.7 ± 0.4[c] | | |

[a]Solvent, MeCN; $T$ = 298 K. [b]Determined by ITC. [c]Determined by UV/vis spectroscopy.

The processing[42−44] of these spectrophotometric data made it possible to carry out an independent determination of the stability constant ($K_a$) for the trisradical tricationic inclusion complex, in addition to affording (Figure 5a) the corresponding electronic spectrum of the 1:1 trisradical tricationic $CBPQT^{2(\bullet+)}\subset MV^{\bullet+}$ complex. It displays the characteristic spectroscopic features of $BIPY^{\bullet+}$ radical−radical interactions (pimerization), namely a broad near-IR band, as well as an increase in the intensities of the absorption bands in the 500−600 nm region compared with the free components dissolved on their own in solution. The results from this titration reveal[45] a $K_a$ value of (7.9 ± 5.5) × $10^4$ $M^{-1}$, an association constant that is consistent within experimental error of that ((5.0 ± 0.6) × $10^4$ $M^{-1}$) determined from the ITC experiments. The thermodynamic parameters obtained from both the ITC and UV/vis spectroscopic data are summarized in Table 1.

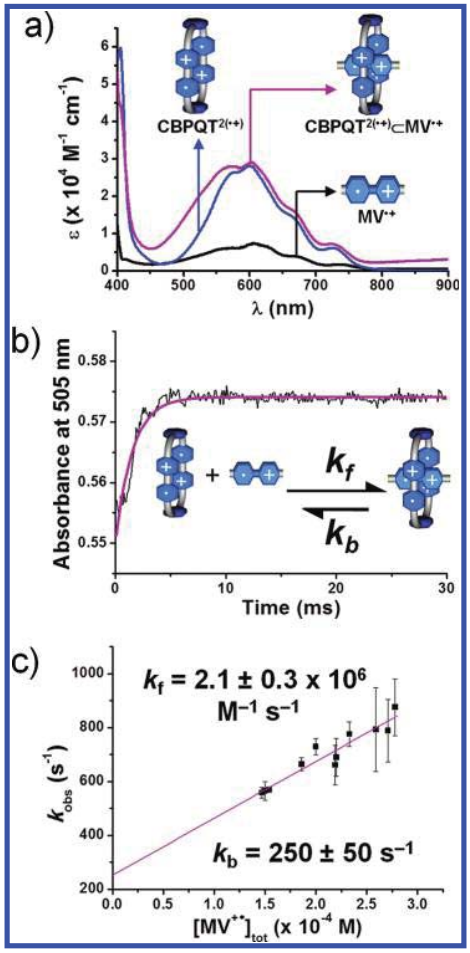


**Figure 5.** (a) UV/vis electronic spectra of $CBPQT^{2(\bullet+)}$, $MV^{\bullet+}$, and $CBPQT^{2(\bullet+)}\subset MV^{\bullet+}$ recorded in MeCN at 298.0(2) K. Formation of the $CBPQT^{2(\bullet+)}\subset MV^{\bullet+}$ inclusion complex is characterized by a broadening of the absorption band centered around 600 nm and formation of a broad band in the NIR. (b) Kinetic trace for the formation of the $CBPQT^{2(\bullet+)}\subset MV^{\bullet+}$ inclusion complex obtained using stopped-flow spectroscopy in MeCN at 298.0(2) K. A single rate-limiting-step is observed. $[CBPQT^{2(\bullet+)}]_0$ = 1.13 × $10^{-5}$ M; $[MV^{\bullet+}]_0$ = 2.18 × $10^{-4}$ M. (c) A plot of the apparent pseudo-first-order rate constant, $k_{obs}$, versus the concentration of $MV^{\bullet+}$, with concentration of $CBPQT^{2(\bullet+)}$ held constant. Solvent, MeCN; $T$ = 298.0(2) K; $[CBPQT^{2(\bullet+)}]_0$ = 1.13 × $10^{-5}$ M.

Stopped-flow UV/vis spectroscopy was performed to evaluate the kinetic parameters controlling the association and dissociation of the trisradical tricationic $CBPQT^{2(\bullet+)}\subset MV^{\bullet+}$ inclusion complex. The absorption at 505 nm was used as a measure of the concentration of the inclusion complex as a function of time, employing pseudo-first-order experimental protocols. A monoexponential increase of the absorbance at 505 nm in the millisecond time range was recorded for the formation of the trisradical trication. From these experiments, a single rate-limiting step (Figure 5b), governing the formation of the inclusion complex, was deduced. The experimental data indicate that the formation of the 1:1 complex proceeds in a single, very fast rate-limiting step. The concentration of $MV^{\bullet+}$ was varied and the corresponding pseudo-first-order rate constant ($k_{obs}$) was shown to depend linearly on $[MV^{\bullet+}]_{tot}$ according to the following equation:

$$k_{obs} = a[MV^{\bullet+}]_{tot} + b$$

The experimental data led us to suggest the following concerted mechanism:

$$CBPQT^{2(\bullet+)} + MV^{\bullet+} \underset{k_b}{\overset{k_f}{\rightleftarrows}} CBPQT^{2(\bullet+)} \subset MV^{\bullet+}$$

where

$$k_{obs} = k_f[MV^{\bullet+}]_{tot} + k_b$$

and $k_f = a$ ($M^{-1}$ $s^{-1}$), the bimolecular association rate constant, and $k_b = b$ ($s^{-1}$), the monomolecular dissociation rate constant.

The fact that the formation of the $CBPQT^{2(\bullet+)}\subset MV^{\bullet+}$ complex proceeds very rapidly ($k_f$ = (2.1 ± 0.3) × $10^6$ $M^{-1}$ $s^{-1}$) in a single rate-limiting step indicates[46] the absence of either strong electrostatic repulsions or steric hindrance at play during this process. A plot of $k_{obs}$ versus the concentration of $MV^{\bullet+}$ yielded (Figure 5c) a rate of association $k_f$ of (2.1 ± 0.3) × $10^6$ $M^{-1}$ $s^{-1}$, and a rate of dissociation $k_b$ of 250 ± 50 $s^{-1}$. The ratio of $k_f/k_b$ (0.84 × $10^4$ $M^{-1}$) is reasonably consistent with the thermodynamic equilibrium constants determined by ITC [(5.04 ± 0.63) × $10^4$ $M^{-1}$] and UV/vis [(7.9 ± 5.5) × $10^4$ $M^{-1}$] spectroscopy. The $k_f$ value obtained for the formation of the trisradical $CBPQT^{2(\bullet+)}\subset MV^{\bullet+}$ complex is an order of magnitude smaller compared[47] with the threading rate constant ($k_f$ = 3.0 ± 0.3) × $10^7$ $M^{-1}$ $s^{-1}$, MeCN, 293 K) for the BHEEN guest entering the cavity of the $CBPQT^{4+}$ ring. The monomolecular dissociation rate constant ($k_b$ = 250 ± 50 $s^{-1}$) for the $CBPQT^{2(\bullet+)}\subset MV^{\bullet+}$ complex is comparable to that ($k_b$ = 530 ± 50 $s^{-1}$, MeCN, 293 K) of the $CPBQT^{4+}\subset$BHEEN


dx.doi.org/10.1021/ja2089603 | J. Am. Chem.Soc. 2012, 134, 3061−3072

complex dissociation rate constant. Although the rate constant for formation of the trisradical $CBPQT^{2(\bullet+)}\subset MV^{\bullet+}$ complex is an order of magnitude less than that for the formation of $CPBQT^{4+}\subset BHEEN$, we have shown previously for the formation[46] of [2]pseudorotaxanes with threads containing 1,5-dioxynaphthalene units together with terminal $BIPY^{2+}$ units flanking either side that the threading of the $CBPQT^{4+}$ ring is slowed ($k_f = (7.0 \pm 0.7) \times 10^{-4}\ M^{-1}\ s^{-1}$, 0.1 M NaCl in $H_2O$, 298 K) by many orders of magnitude as a consequence of the $BIPY^{2+}$ units serving the role of electrostatic barriers.

**Cyclic Voltammetry and Digital Simulations.** In a 1:1 mixture of $CBPQT^{4+}$ and $MV^{2+}$, both in their fully oxidized forms, no binding between the two charged species is observed, presumably as a consequence of their similar $\pi$-electron-poor electronic characteristics, not to mention electrostatic repulsion. Upon a three-electron reduction, wherein two electrons contribute to the formation of the $CBPQT^{2(\bullet+)}$ ring and one to the formation of the $MV^{\bullet+}$ guest, production of the trisradical $CBPQT^{2(\bullet+)}\subset MV^{\bullet+}$ inclusion complex ensues as a result of favorable radical−radical interactions, all of which can be stimulated electrochemically. The nature of these radical−radical interactions is largely a consequence of radical pairing, a phenomenon that has been studied[21c] in considerable detail in the case of the classical viologen radical cation dimers and violenes in general.[48] When viologen radical cations dimerize, at distances defined by van der Waals contacts, the dimers become radically paired and hence EPR silent (inactive), while the viologen radical cation monomer results in a characteristic signal. This mechanism involving radical pairing has important implications when considering the electrochemical behavior of the trisradical $CBPQT^{2(\bullet+)}\subset MV^{\bullet+}$ complex. Consider the hypothesis where only two of the $BIPY^{\bullet+}$ radical cation subunits of the complex are paired at any one time, leaving one $BIPY^{\bullet+}$ radical cation subunit of the $CBPQT^{2(\bullet+)}$ ring unpaired. One might anticipate that this unpaired $BIPY^{\bullet+}$ unit would not be as strongly engaged in radical−radical interactions as the other two paired $BIPY^{\bullet+}$ units. Theoretical investigations, based on DFT to calculate the SOMO of the trisradical $CBPQT^{2(\bullet+)}\subset MV^{\bullet+}$ complex, support[26a] this hypothesis (*vide supra*), by revealing that orbital overlap of the $MV^{\bullet+}$ guest occurs predominantly with only one of the $BIPY^{\bullet+}$ units in the $CBPQT^{2(\bullet+)}$ ring. The fact that one of the two $BIPY^{\bullet+}$ radical cations in the ring is not as strongly interactive with the $MV^{\bullet+}$ guest mandates, from a thermodynamic perspective, that this unpaired $BIPY^{\bullet+}$ unit undergoes reduction to its neutral $BIPY^0$ form at a less negative potential, that is, it should be easier to reduce in comparison with the two radically paired $BIPY^{\bullet+}$ units. The corollary to this argument is that the reoxidation of the unpaired $BIPY^{\bullet+}$ radical cation unit should also occur at less positive potentials, that is, it should be easier to oxidize, compared with the two paired $BIPY^{\bullet+}$ radical cation units. It follows therefore that the formation of a tetracationic $CBPQT^{(2+)(\bullet+)}\subset MV^{\bullet+}$ bisradical inclusion complex must appear in any discussion of the electrochemical switching mechanism.

The CV of an equimolar mixture of the $CBPQT^{4+}$ ring and $MV^{2+}$ is presented in Figure 6a. The first reduction peak (−0.32 V, peak potential) is a three-electron process with two electrons going to $CBPQT^{4+}$, forming the diradical dication $CBPQT^{2(\bullet+)}$, and one electron going to $MV^{2+}$, forming the radical cation $MV^{\bullet+}$. As a consequence of this three-electron process, formation of the trisradical tricationic $CBPQT^{2(\bullet+)}\subset MV^{\bullet+}$ inclusion complex ensues spontaneously. The result of this inclusion is that only one of the $BIPY^{\bullet+}$ radical cations of the complexed $CBPQT^{2(\bullet+)}$ interacts strongly with the $MV^{\bullet+}$ radical cation, leading to the fact that the second reduction of this weakly interacting, unpaired $BIPY^{\bullet+}$ occurs at a less negative potential (−0.76 V, peak potential), roughly at the same potential as the second reduction of $CBPQT^{4+}$ alone in solution. The reduction of the paired $BIPY^{\bullet+}$ units of the complexed $CBPQT^{2(\bullet+)}$ and the $MV^{\bullet+}$ radical cation, occur

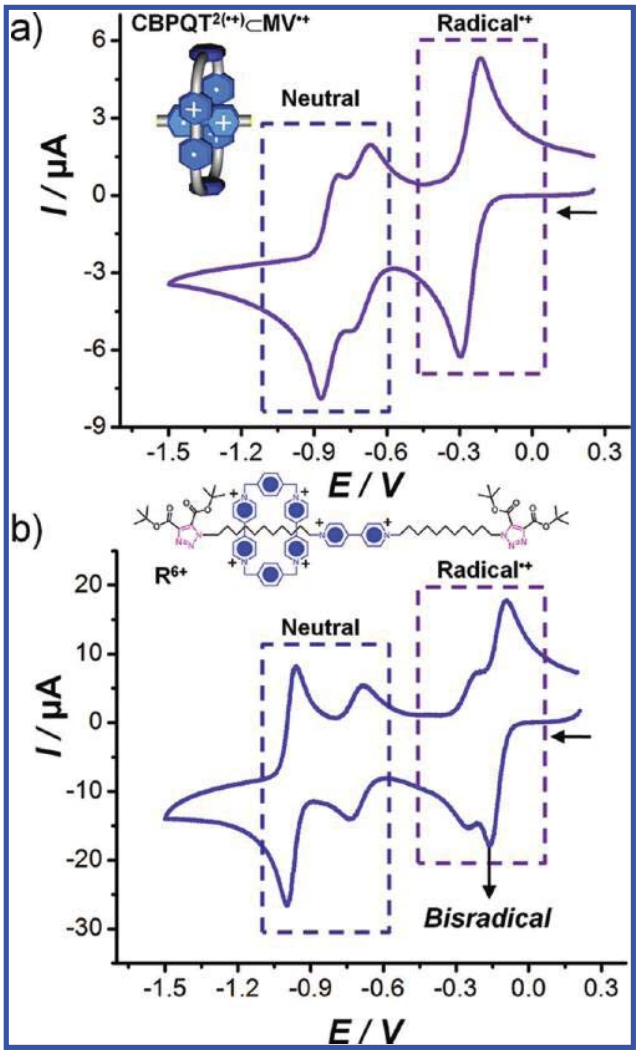


**Figure 6.** (a) Cyclic voltammogram of an equimolar mixture of $CBPQT^{4+}$ and $MV^{2+}$ in MeCN at 1.0 mM. The first reduction process is a three-electron one leading to the formation of the trisradical $CBPQT^{2(\bullet+)}\subset MV^{\bullet+}$ inclusion complex. As a consequence of radical pairing between one $BIPY^{\bullet+}$ of the ring and that from $MV^{\bullet+}$, the reduction of the complex to its neutral form is observed to occur over, first by a one-electron process, followed by a two-electron one, the former (and less negative) one is assigned to the reduction of the unpaired $BIPY^{\bullet+}$ unit in the ring. (b) Cyclic voltammogram of the [2]rotaxane $R^{6+}$ containing only a $BIPY^{2+}$ recognition unit in its dumbbell component. As a consequence of both radical pairing and the mechanical bond, the first reduction process leading to the trisradical species $R^{3(\bullet+)}$ is observed to occur over, first by a two-electron followed by a one-electron process. The first two-electron process is assigned to the simultaneous reduction of one $BIPY^{2+}$ unit of the ring and the $BIPY^{2+}$ unit of the dumbbell component, leading to the formation of a stable bisradical intermediate. Both voltammograms were recorded at a scan rate of 200 mV $s^{-1}$ with an Ag/AgCl reference electrode.


dx.doi.org/10.1021/ja2089603 | J. Am. Chem.Soc. 2012, 134, 3061−3072

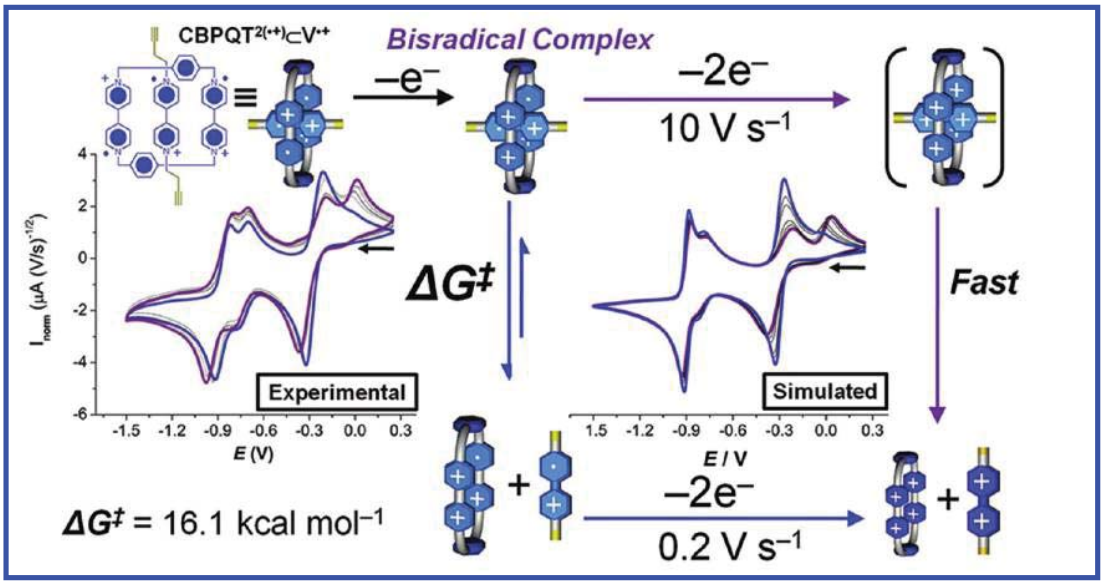


**Figure 7.** Experimental and simulated variable scan rate cyclic voltammograms of a 1:1 mixture of $CBPQT^{4+}$ and $V^{2+}$ in MeCN at 298 K. As a consequence of radical pairing, one of the $BIPY^{\bullet+}$ radical cation units is oxidized first (at a less positive potential) during the scan, leading to the formation of the bisradical $CBPQT^{(2+)(\bullet+)}\subset V^{\bullet+}$ intermediate. The presence of the $BIPY^{2+}$ unit in the ring $CBPQT^{(2+)(\bullet+)}$ ring leads to dissociation of the complex observable on the time scale of the CV experiments. When the experimental data were fitted to the digital simulations, the free energy barrier, $\Delta G^{\ddagger}$, to dissocation of the bisradical $CBPQT^{(2+)(\bullet+)}\subset V^{\bullet+}$ complex was determined to be 16.1 kcal $mol^{-1}$. Blue trace = 200 mV $s^{-1}$; purple trace =10 V $s^{-1}$. IR compensation was applied and an Ag/AgCl reference electrode was used.

simultaneously at a more negative potential (−0.87 V, peak potential) as a two-electron process.

The [2]rotaxane $R^{6+}$ (Figure 6b, top), composed of a $CBPQT^{4+}$ ring mechanically interlocked around a dumbbell containing a $BIPY^{2+}$ unit, was obtained using a threading-followed-by-stoppering template-directed protocol[26b] relying upon radical−radical interactions and employing a copper-free 1,3-dipolar cycloaddition in the final reaction step, thus forming the mechanical bond. The mechanical bond dictates that the $CBPQT^{4+}$ ring cannot escape the influence of the $BIPY^{2+}$ unit in the dumbbell component entirely. In this situation, *both* the *trisradical* and *bisradical* forms of the rotaxane are stable species! Electrochemical experiments reveal that reduction of $R^{6+}$ to the trisradical tricationic form $R^{3(\bullet+)}$ occurs over two different electron-transfer processes. The first is a two-electron reduction process, which is assigned to the formation of the paired $BIPY^{\bullet+}$ radical cations of the dumbbell with one from the ring forming the bisradical tetracationic $R^{(2+)2(\bullet+)}$. The subsequent one-electron transfer is assigned to the reduction of the remaining unpaired $BIPY^{2+}$ in the $CBPQT^{(2+)(\bullet+)}$ ring, a process that generates the trisradical tricationic $R^{3(\bullet+)}$ form of the [2]rotaxane. Both of these redox processes are independent of the scan rate (50−1000 mV $s^{-1}$, Supporting Information), that is, they are totally reversible because the mechanical bond excludes the possibility of dissociation and so serves to stabilize the bisradical form of the rotaxane in comparison with that of its bisradical tetracationic $CBPQT^{(2+)(\bullet+)}\subset MV^{\bullet+}$ supramolecular analogue.

In an effort to detect the bisradical tetracationic $CBPQT^{(2+)(\bullet+)}\subset MV^{\bullet+}$ inclusion complex, variable scan rate CV experiments were carried out initially on a 1:1 mixture of $CBPQT^{4+}$ and $MV^{2+}$. They reveal (Supporting Information), however, that the reoxidation of the trisradical tricationic complex $CBPQT^{2(\bullet+)}\subset MV^{\bullet+}$ is independent of scan rate[49] (up to 30 V $s^{-1}$). This observation suggests that dissociation of $CBPQT^{(2+)(\bullet+)}\subset MV^{\bullet+}$ is too fast to detect on the time scale of the CV experiments. In order to probe the nature of the bisradical tetracationic intermediate, we performed variable scan rate CV experiments on a 1:1 mixture of $CBPQT^{4+}$ and $V^{2+}$, where the butynyl functional groups of $V^{2+}$ act to slow the rate of dissociation such that the intermediate can be more readily observed under the experimental conditions employed. We hypothesize that the extra steric bulk or favorable noncovalent bonding interactions resulting from the presence of the butynyl substituents of $V^{2+}$ act to stabilize the bisradical tetracationic intermediate, $CBPQT^{(2+)(\bullet+)}\subset V^{\bullet+}$, kinetically by comparison with the methyl groups of $MV^{2+}$.

Evidence for the existence of the $CBPQT^{(2+)(\bullet+)}\subset V^{\bullet+}$ inclusion complex in solution can be obtained (Figure 7) from variable scan rate CV in MeCN. As a consequence of the presence of the dicationic $BIPY^{2+}$ unit, the bisradical $CBPQT^{(2+)(\bullet+)}\subset V^{\bullet+}$ complex forfeits a substantial amount of stability compared with that of the trisradical $CBPQT^{2(\bullet+)}\subset V^{\bullet+}$ complex. The bisradical complex begins to dissociate into its individual components, making reoxidation of the two remaining $BIPY^{\bullet+}$ radical cations of the separate host and guest components occur at a less positive redox potential (approximately −0.35 V), that is, easier to reoxidize. When the scan is performed at a rate slower than the time scale of the dissociation of the $CBPQT^{(2+)(\bullet+)}\subset V^{\bullet+}$ complex, reoxidation of the trisradical tricationic complex is observed to occur as a single, broad oxidation wave. When the reoxidation is performed at progressively faster scan rates, eventually reaching a point where dissociation of the $CBPQT^{(2+)(\bullet+)}\subset V^{\bullet+}$ is slow on the CV time scale, reoxidation of the trisradical tricationic complex is observed to occur by means of (i) a one-electron transfer, followed (ii) by another two-electron transfer, the latter of which occurs at a potential shifted to almost 0 V! The first one-electron oxidation, leading to the formation of $CBPQT^{(2+)(\bullet+)}\subset V^{\bullet+}$, is assignable to the unpaired $BIPY^{\bullet+}$ subunit of the trisradical trication complex, which is more weakly engaged in radical−radical interactions. The second,


dx.doi.org/10.1021/ja2089603 | J. Am. Chem.Soc. 2012, 134, 3061−3072

Table 2. Kinetic Parameters Associated with the Formation of the Trisradical Inclusion Complex between the Diradical Dication $CBPQT^{2(\bullet+)}$ Ring and the Radical Cation $MV^{\bullet+}$ and the Bisradical Complex of $CBPQT^{(2+)(\bullet+)}$ with $V^{\bullet+}$[a]

| | $k_f$, $10^4$ $M^{-1}$ $s^{-1}$ | $k_b$, $s^{-1}$ | $\Delta G_f^{\ddagger}$, kcal $mol^{-1}$ | $\Delta G_b^{\ddagger}$, kcal $mol^{-1}$ |
|---|---|---|---|---|
| $CBPQT^{2(\bullet+)}\subset MV^{\bullet+}$ | 210 ± 30[b] | 250 ± 50[b] | 8.8 ± 0.1[b] | 14.2 ± 0.1[b] |
| $CBPQT^{(2+)(\bullet+)}\subset V^{\bullet+}$ | 6.6 ± 1[c] | 10 ± 2[c] | 11.0 ± 0.7[c] | 16.1 ± 0.5[c] |
| | | 5.0 ± 1.0[d] | | 16.5 ± 1.0[d] |

[a]Solvent, MeCN; $T$ = 298 K. [b]Determined by stopped-flow spectroscopy. [c]Determined by cyclic voltammetry fitted to digitally simulated data. [d]Determined by cyclic voltammetry using a relative integration analysis.

dramatically shifted two-electron process can be assigned to the simultaneous two-electron oxidation of the radically paired $BIPY^{\bullet+}$ units of $CBPQT^{(2+)(\bullet+)}\subset V^{\bullet+}$, leading to the fully oxidized and highly unstable hexacationic $CBPQT^{4+}\subset V^{2+}$ complex, which quickly dissociates on the time scale of the CV experiment.

Because of the dissociation of the $CBPQT^{(2+)(\bullet+)}\subset V^{\bullet+}$ inclusion complex, we hypothesize that the reoxidation potentials for both separated components become shifted toward less positive potentials, resembling those of the free components alone in solution, than the first one-electron oxidation of the unpaired $BIPY^{\bullet+}$ radical cation in the scan, resulting in a single broad reoxidation peak. Mechanistically, we propose a first-order rate law for the dissociation of the $CBPQT^{(2+)(\bullet+)}\subset V^{\bullet+}$ inclusion complex into its individual components that is proportional to a rate constant and the concentration of the bisradical species.

Digital CV simulations of the proposed mechanism were performed (Figure 7) based on the results obtained from ITC and stopped-flow spectroscopy and are in good agreement with the experimental data. Comparisons between digital simulations and the experimental data using a $X^2$ fitting algorithm or by employing a relative integration analysis (see Supporting Information) of the reoxidation waves as a function of time (scan rate) establish the barrier $\Delta G_b^{\ddagger}$ governing the first-order dissociation of the bisradical tetracationic complex to be 16.1 or 16.5 kcal $mol^{-1}$, respectively, at room temperature. Table 2 summarizes the kinetic parameters obtained from stopped-flow UV/vis spectroscopic and CV data. It is worth noting that, since the kinetic reoxidation pathway of the trisradical tricationic complex is scan-rate dependent, it represents an example of a *bilabile* system.[50]

## CONCLUSIONS

As might be inferred by the fact that radically-based switching motifs are being integrated into host–guest and mechanically interlocked systems in only recent times, perhaps a prejudice against organic radicals as being useful building blocks in these contexts exists. Under appropriate conditions, we have shown[26b] that it is possible to take advantage of favorable radical–radical interactions in order to template the synthesis of MIMs, as well as to induce them to switch[26a,c] from one recognition unit to another in a reversible fashion. In the research reported in this paper, we investigated the thermodynamics and kinetics, as well as the overall electrochemical mechanism, of the formation of the trisradical inclusion complex whereby $CBPQT^{4+}$ encircles $MV^{2+}$ after reduction of each $BIPY^{2+}$ species to their respective radical cations. Solid-state superstructural analysis confirms predictions that the $MV^{\bullet+}$ radical cation resides in a centrosymmetric fashion inside the cavity of the $CBPQT^{2(\bullet+)}$ ring. Further inspection of solid-state superstructure beyond the 1:1 complex reveals an infinite $BIPY^{\bullet+}$ radical cation stack of adjacent $CBPQT^{2(\bullet+)}\subset MV^{\bullet+}$ inclusion complexes. The electrochemical mechanism for formation and dissociation of the inclusion complex has been elucidated using CV, ITC, UV/vis, and stopped-flow spectroscopy. Variable scan rate CV reveals that the reoxidation pathway of the trisradical tricationic complex occurs through a bisradical tetracationic intermediate, which can be detected when the dibutynyl viologen, $V^{\bullet+}$, is employed as the guest. We speculate that such a bisradical tetracationic complex, having both a $BIPY^{\bullet+}$ radical cation and a dicationic $\pi$-electron-poor $BIPY^{2+}$ unit in the ring component, might possess "amphiphilic" behavior, that is, it can be both donor-loving and radical-loving. Such a property could clearly be harnessed in the context of MIMs in order to achieve more sophisticated control of their relative intramolecular motions. Greater control of the relative motions of MIMs will provide chemists with an enhanced ability to design and synthesize complex integrated systems.[51]

## EXPERIMENTAL SECTION

**General Methods.** The tetracationic cyclophane, cyclobis (paraquat-*p*-phenylene) tetrakishexafluorophosphate[11] (CBPQT·$4PF_6$), the dimethyl viologen[21c] (MV·$2PF_6$), and the dibutynyl viologen[52] (V·$2PF_6$), as well as the single-station [2]rotaxane[26b] (R·$6PF_6$) were all prepared according to literature procedures. Zinc dust was activated by stirring it with dilute HCl during 10–15 min and then washing it several times with distilled $H_2O$, EtOH, and absolute $Et_2O$ before drying rigorously. This procedure removes oxides, which form slowly upon standing in air from the surface of zinc.[53] All the physicochemical investigations were carried out with spectroscopic grade MeCN (Acros Organics ≥99.9% for spectroscopy). The stock solutions of CBPQT·$4PF_6$ and MV·$2PF_6$ were prepared by weighing using an AG 245 Mettler Toledo analytical balance (precision 0.01 mg). Complete dissolution of CBPQT·$4PF_6$ and MV·$2PF_6$ in MeCN was achieved using an ultrasonic bath (Bandelin Sonorex RK102 Transistor). The concentrations were thus obtained by weighing the appropriate amounts. Reduction of $CBPQT^{4+}$ and $MV^{2+}$ into the corresponding diradical dication $CBPQT^{2(\bullet+)}$and radical cation $MV^{\bullet+}$ was achieved under argon ($CO_2$- and $O_2$-free argon using a Sigma Oxiclear cartridge) in less than 1 h by vigorous stirring with activated zinc dust. The formation of the radicals were monitored (see Supporting Information) by absorption spectrophotometry. Isothermal titration calorimetry (ITC) experiments were performed on a MicroCal system, VP-ITC model. Cyclic voltammetry (CV) was carried out at room temperature in argon-purged MeCN solutions with a Gamry Multipurpose instrument (reference 600) interfaced to a PC. The CV experiments were performed using a glassy carbon working electrode (0.071 $cm^2$, BASi). The electrode surface was polished routinely with 0.05 $\mu$m alumina–water slurry on a felt surface immediately before use. The counter electrode was a Pt coil, and the reference electrode was a Ag/AgCl electrode, unless otherwise noted. The concentrations of the sample and supporting electrolyte, tetrabutylammonium hexafluorophosphate (TBA·$PF_6$), were $1.0 \times 10^{-3}$ $M^{-1}$ and 0.1 $M^{-1}$, respectively. Experimental error of potential values was ±10 mV. All simulations of electrochemical data were performed using DigiSim.

**UV/Vis Absorption Spectrophotometric Titration.** A solution (50 mL) of CBPQT·$4PF_6$ ($4.36 \times 10^{-5}$ M) was introduced into a

jacketed cell (Metrohm) maintained at 25.0(2) °C (Lauda E200/O11 thermostat) while being deoxygenated continuously by $CO_2$- and $O_2$-free argon. In the first instance, an absorption spectrum was recorded using a Varian Cary 50 spectrophotometer, fitted with Hellma optical fibers (Hellma, 041.002-UV), and an immersion probe made of quartz suprazil (Hellma, 661.500-QX). Activated zinc dust was then added, and the formation of the diradical dication $CBPQT^{2(\bullet+)}$ was monitored by recording the absorption spectra as a function of time until complete reduction was achieved (~1 h). Concomitantly, a stock MeCN solution of $MV^{\bullet+}$ ($3.35 \times 10^{-3}$ M, 10 mL) was prepared from $MV{\cdot}2PF_6$ under the same conditions, that is, continuous deoxygenation with $CO_2$- and $O_2$-free argon and vigorous stirring in the presence of activated zinc dust. Microvolumes of concentrated MeCN solutions of the radical cation $MV^{\bullet+}$ were added to a MeCN solution of $CBPQT^{2(\bullet+)}$, and the reaction was allowed to stand for 15 min with vigorous stirring in the presence of activated zinc dust and under anaerobic conditions to ensure that both the complete reduction of the $BIPY^{2+}$ derivatives and the host–guest association equilibration were attained. After each addition, a UV/vis spectrum was recorded from 230 to 900 nm on the Cary 50 (Varian) spectrophotometer maintained at 25(2) °C. The ratio $[MV^{\bullet+}]_{tot}/[CBPQT^{2(\bullet+)}]_{tot}$ was varied (see the Supporting Information) from 0 to 4.38. The spectrophotometric data were analyzed with the Specfit program, which adjusts the absorptivities and the stability constants of the species formed at equilibrium. Specfit uses factor analysis to reduce the absorbance matrix and extract the eigenvalues prior to the multi-wavelength fit of the reduced data set according to the Marquardt algorithm.

**Formation Kinetics.** The formation kinetics of the trisradical inclusion complex $CBPQT^{2(\bullet+)}\subset MV^{\bullet+}$ were measured on a SX-18MV stopped-flow spectrophotometer from Applied Photophysics. The temperature was maintained at 25.0(2) °C with the help of a Lauda E200/RE220 cryothermostat, and the formation kinetics of the trisradical species was monitored at $\lambda$ = 505 nm ($l$ = 1 cm), a wavelength that corresponds to the maximum of absorbance difference between the reactants ($MV^{\bullet+}$ and $CBPQT^{2(\bullet+)}$) and the product ($CBPQT^{2(\bullet+)}\subset MV^{\bullet+}$) within the spectroscopic window employed under the experimental conditions. The $CBPQT^{4+}$ concentration was fixed at $1.13 \times 10^{-5}$ M, and the range of $MV^{2+}$ concentrations was varied from $1.47 \times 10^{-4}$ to $2.78 \times 10^{-4}$ M by dilution of a concentrated stock solution. At least 10 times more concentrated solutions of $MV^{2+}$ with respect to $CBPQT^{4+}$ were used in order to impose pseudo-first-order conditions. Each solution, namely, the $CBPQT^{4+}$ and the $MV^{2+}$ samples, was reacted with activated zinc dust during more than 1 h to ensure complete reduction into $CBPQT^{2(\bullet+)}$ and $MV^{\bullet+}$species. The data sets, averaged out of at least three replicates, were recorded and analyzed with the commercial software Biokine.[54] This program fits up to three exponential functions to the experimental curves with the Simplex algorithm[55] after initialization with a Padé–Laplace method.[56]

## ■ ASSOCIATED CONTENT

### Ⓢ Supporting Information

Further details and characterization by $^1$H DOSY NMR, CV, digital CV simulations, X-ray crystallography, ITC, and UV/vis spectroscopy. This material is available free of charge via the Internet at http://pubs.acs.org.

## ■ AUTHOR INFORMATION


### Corresponding Author

elhabiri@chimie.u-strasbg.fr; stoddart@northwestern.edu


## ■ ACKNOWLEDGMENTS


We (A.C.F., J.C.B., H.L., A.C., J.J.G., Z.L., and J.F.S.) at Northwestern University acknowledge support from the Air Force Office of Scientific Research (AFSOR) under the Multidisciplinary Research Program of the University Research Initiative (MURI) Award FA9550-07-1-0534 on "Bioinspired Supramolecular Enzymatic Systems" and the National Science Foundation (NSF) under the auspices of Award CHE-0924620. We (W.A.G and J.F.S.) also acknowledge support by the Microelectronics Advanced Research Corporation (MARCO) and its Focus Center Research Program (FCRP) on Functional Engineered NanoArchitectonics (FENA) as well as support from the Non-Equilibrium Energy Research Center (NERC), which is an Energy Frontier Research Center (EFRC) funded by the U.S. Department of Energy, Office of Basic Sciences (DOE-BES), under Award DE-SC0000989. W.A.G., J.F.S., A.C.F., and J.C.B. were supported by the WCU Program (NRF R-31-2008-000-10055-0) funded by the Ministry of Education, Science and Technology, Korea. A.C.F. acknowledges support from an NSF Graduate Research Fellowship. This work was also supported (M.E. and D.A.L.) by the Centre National de la Recherche Scientifique (CNRS) and the University of Strasbourg (UMR 7509 CNRS-UdS) in France.


## ■ REFERENCES


(1) Stoddart, J. F.; Colquhoun, H. M. *Tetrahedron* **2008**, *64*, 8231.

(2) (a) Nakahara, A.; Wang, J. H. *J. Phys. Chem.* **1963**, *67*, 496. (b) Monk, P. M. S.; Hodgkinson, N. M.; Partridge, R. D. *Dyes Pigm.* **1999**, *43*, 241.

(3) (a) Pedersen, C. J. *J. Am. Chem. Soc.* **1967**, *89*, 2495. (b) Pedersen, C. J. *Aldrichimica Acta* **1971**, *4*, 1.

(4) (a) Pedersen, C. J. *J. Am. Chem. Soc.* **1970**, *92*, 386. (b) Bright, D.; Truter, M. R. *J. Chem. Soc. B* **1970**, 1544. (c) Bush, M. A.; Truter, M. R. *J. Chem. Soc. B* **1971**, 1440. (d) Frensdorff, H. K. *J. Am. Chem. Soc.* **1971**, *93*, 600. (e) Bush, M. A.; Truter, M. R. *J. Chem. Soc., Perkin Trans. 2* **1972**, 341. (f) Mallinson, P. R.; Truter, M. R. *J. Chem. Soc. Perkin Trans. 2* **1972**, 1818. (g) Pedersen, C. J.; Frensdorff, H. K. *Angew. Chem., Int. Ed.* **1972**, *11*, 16.

(5) Pedersen, C. J. *Angew. Chem., Int. Ed. Engl.* **1988**, *27*, 1021.

(6) (a) Cram, D. J.; Cram, J. M. *Science* **1971**, *183*, 803. (b) Cram, D. J. *Science* **1983**, *219*, 1177. (c) Cram, D. J.; Cram, J. M. *Container Molecules and Their Guests*; Royal Society of Chemistry: Cambridge, U.K., 1994.

(7) Cram, D. J. *Angew. Chem., Int. Ed. Engl.* **1988**, *27*, 1009.

(8) (a) Lehn, J.-M. *Supramolecular Chemistry Concepts and Perspectives*; Wiley-VCH: Weinheim, Germany, 1995. (b) Beer, P. D.; Gale, P. A.; Smith, D. K. *Supramolecular Chemistry*; Oxford University Press: Oxford, U.K., 1999. (c) Steed, J. W.; Atwood, J. L. *Supramolecular Chemistry*; Wiley-VCH: Weinheim, Germany, 2009. (d) Stoddart, J. F. *Nat. Chem.* **2009**, *1*, 14.

(9) (a) Lehn, J.-M. *Science* **1985**, *227*, 849. (b) Lehn, J.-M. *Angew. Chem., Int. Ed. Engl.* **1988**, *27*, 89. (c) Lehn, J.-M. *Angew. Chem., Int. Ed. Engl.* **1990**, *29*, 1304.

(10) (a) Allwood, B. L.; Shahriari-Zaverah, H.; Stoddart, J. F.; Williams, D. J. *J. Chem. Soc., Chem. Commun.* **1987**, 1058. (b) Ashton, P. R.; Chrystal, E. J. T.; Mathias, J. P.; Parry, K. P.; Slawin, A. M. Z.; Spencer, N.; Stoddart, J. F.; Williams, D. J. *Tetrahedron Lett.* **1987**, *28*, 6367. (c) Gasa, T. B.; Spruell, J. M.; Dichtel, W. R.; Sørensen, T. J.; Philp, D.; Stoddart, J. F.; Kuzmič, P. *Chem.—Eur. J.* **2009**, *15*, 106. (d) Trabolsi, A.; Fahrenbach, A. C.; Dey, S. K.; Share, A. I.; Friedman, D. C.; Basu, S.; Gasa, T. B.; Khashab, N. M.; Saha, S.; Aprahamian, I.; Khatib, H. A.; Flood, A. H.; Stoddart, J. F. *Chem. Commun.* **2010**, *46*, 871.

(11) (a) Odell, B.; Reddington, M. V.; Slawin, A. M. Z.; Spencer, N.; Stoddart, J. F.; Williams, D. J. *Angew. Chem., Int. Ed. Engl.* **1988**, *27*, 1547. (b) Asakawa, M.; Dehaen, W.; L'abbé, G.; Menzer, S.; Nouwen, J.; Raymo, F. M.; Stoddart, J. F.; Williams, D. J. *J. Org. Chem.* **1996**, *61*, 9591. (c) Chiang, P.-T.; Cheng, P.-N.; Lin, C.-F.; Liu, Y.-H.; Lai, C.-C.; Reng, S.-M.; Chiu, S.-H. *Chem.—Eur. J.* **2006**, *12*, 865. (d) Sue, C.-H.; Basu, S.; Fahrenbach, A. C.; Shveyd, A. K.; Dey, S. K.; Botros, Y. Y.; Stoddart, J. F. *Chem. Sci.* **2010**, *1*, 119. (e) Boyle, M. M.; Forgan, R. S.; Friedman, D. C.; Gassensmith, J. J.; Smaldone, R. A.; Stoddart, J. F.; Sauvage, J.-P. *Chem. Commun.* **2011**, *47*, 11870.

(12) For a recent paper that covers the literature extensively, see: Basu, S.; Coskun, A.; Friedman, D. C.; Olson, M. A.; Benítez, D.; Tkatchouk, E.; Barin, G.; Yang, J.; Fahrenbach, A. C.; Goddard, W. A. III; Stoddart, J. F. *Chem.—Eur. J.* **2011**, *17*, 2107.
(13) (a) Stoddart, J. F. *Chem. Soc. Rev.* **2009**, *38*, 1802. (b) Coskun, A.; Banaszak, M.; Astumian, R. D.; Stoddart, J. F.; Grzybowski, B. A. *Chem. Soc. Rev.* **2012**, *41*, 19.
(14) (a) Olson, M. A.; Botros, Y. Y.; Stoddart, J. F. *Pure Appl. Chem.* **2010**, *82*, 1569. (b) Wang, C.; Olson, M. A.; Fang, L.; Benítez, D.; Tkatchouk, E.; Basu, S.; Zhang, D.; Zhu, Z.; Goddard, W. A. III; Stoddart, J. F. *Proc. Natl. Acad. Sci. U.S.A.* **2010**, *107*, 13991.
(15) (a) Ashton, P. R.; Goodnow, T. T.; Kaifer, A. E.; Reddington, M. V.; Slawin, A. M. Z.; Spencer, N.; Stoddart, J. F.; Vicent, C.; Williams, D. J. *Angew. Chem., Int. Ed. Engl.* **1989**, *28*, 1396. (b) Asakawa, M.; Ashton, P. R.; Balzani, V.; Credi, A.; Hamers, C.; Mattersteig, G.; Montalto, M.; Shipway, A. N.; Spencer, N.; Stoddart, J. F.; Tolley, M. S.; Venturi, M.; White, A. J. P.; Williams, D. J. *Angew. Chem., Int. Ed.* **1998**, *37*, 333. (c) Cao, D.; Amelia, M.; Klivansky, L. M.; Koshkakaryan, G.; Khan, S. I.; Semeraro, M.; Silvi, S.; Venturi, M.; Credi, A; Liu, Y. *J. Am. Chem. Soc.* **2010**, *132*, 1110. (d) Fang, L.; Basu, S.; Sue, C.-H.; Fahrenbach, A. C.; Stoddart, J. F. *J. Am. Chem. Soc.* **2011**, *133*, 396. (e) Forgan, R. S.; Sauvage, J.-P.; Stoddart, J. F. *Chem. Rev.* **2011**, *111*, 5434.
(16) (a) Anelli, P. L.; Spencer, N.; Stoddart, J. F. *J. Am. Chem. Soc.* **1991**, *113*, 5131. (b) Bissell, R. A.; Córdova, E.; Kaifer, A. E.; Stoddart, J. F. *Nature* **1994**, *369*, 133. (c) Tseng, H.-R.; Vignon, S. A.; Stoddart, J. F. *Angew. Chem. Int. Ed.* **2003**, *42*, 1491. (d) Dey, S. K.; Coskun, A.; Fahrenbach, A. C.; Barin, G.; Basuray, A. N.; Trabolsi, A.; Botros, Y. Y.; Stoddart, J. F. *Chem. Sci.* **2011**, *2*, 1046.
(17) (a) Flood, A. H.; Stoddart, J. F.; Steverman, D. W.; Heath, J. R. *Science* **2004**, *306*, 2055. (b) Heath, J. R. *Annu. Rev. Mater. Res.* **2009**, *39*, 1. (c) van der Molen, S. J.; Liljeroth, P. *J. Phys.: Condens. Matter* **2010**, *22*, No. 133001.
(18) (a) Collier, C. P.; Mattersteig, G.; Wong, E. W.; Luo, Y.; Beverly, K.; Sampaio, J.; Raymo, F. M.; Stoddart, J. F.; Heath, J. R. *Science* **2000**, *289*, 1172. (b) Lou, Y.; Collier, C. P.; Jeppesen, J. O.; Nielson, K. A.; DeIonno, E.; Ho, G.; Perkins, J.; Tseng, H.-R.; Yamamoto, T.; Stoddart, J. F.; Heath, J. R. *ChemPhysChem* **2002**, *3*, 519. (c) Green, J. E.; Choi, J. W.; Boukai., A.; Bunimovich, Y.; Johnston-Halperin, E.; DeIonno, E.; Luo, Y.; Sheriff, B. A.; Xu, K.; Shin, Y. S.; Tseng, H.-R.; Stoddart, J. F.; Heath, J. R. *Nature* **2007**, *445*, 414. (d) Zhang, W.; DeIonno, E.; Dichtel, W. R.; Fang, L.; Trabolsi, A.; Olsen, J.-C.; Benítez, D.; Heath, J. R.; Stoddart, J. F. *J. Mater. Chem.* **2011**, *21*, 1487.
(19) (a) Liu, Y.; Flood, A. H.; Bonvallet, P. A.; Vignon, S. A.; Northrop, B. H.; Tseng, H.-R.; Jeppesen, J. O.; Huang, T. J.; Brough, B.; Baller, M.; Magonov, S.; Solares, S. D.; Goddard, W. A. III; Ho, C.-M.; Stoddart, J. F. *J. Am. Chem. Soc.* **2005**, *127*, 9745. (b) Juluri, B. K.; Kumar, A. S.; Liu, Y.; Ye, T.; Yang, Y.-W.; Flood, A. H.; Fang, L.; Stoddart, J. F.; Weiss, P. S.; Huang, T. J. *ACS Nano* **2009**, *3*, 291.
(20) (a) Cotí, K. K.; Belowich, M. E.; Liong, M.; Ambrogio, M. W.; Lau, Y. A.; Khatib, H. A.; Zink, J. I.; Kashab, N. M.; Stoddart, J. F. *Nanoscale* **2009**, *1*, 16. (b) Ambrogio, M. W.; Thomas, C. R.; Zhao, Y.-L.; Zink, J. I.; Stoddart, J. F. *Acc. Chem. Res.* **2011**, *44*, 903.
(21) (a) Michaelis, L.; Hill, E. S. *J. Gen. Physiol.* **1933**, *16*, 859. (b) Michaelis, L. *Chem. Rev.* **1935**, *16*, 243. (c) Bird, C. L.; Kuhn, A. T. *Chem. Soc. Rev.* **1981**, *10*, 49. (c) Monk, P. M. S. *The Viologens: Physicochemical Properties, Synthesis and Applications of the Salts of 4,4′-Bipyridine*; Wiley: New York, 1998.
(22) W. M. Schwarz investigated solutions of viologen radical cations over the concentration range in which an obvious color change is observed and provided evidence for the idea that a monomer−dimer equilibrium is responsible for the color change. Kosower references the 1961 thesis of Schwarz at the University of Wisconsin archive as the starting point for the establishment of the monomer−dimer equilibrium hypothesis. Kosower, E. M.; Cotter, J. L. *J. Am. Chem. Soc.* **1964**, *86*, 5524.
(23) (a) Evans, A. G.; Evans, J. C.; Baker, M. W. *J. Chem. Soc., Perkin Trans.* **1975**, *2*, 1310. (b) Bruinink, J.; Kregting, C. G. A.; Panjeé, J. J. *J. Electrochem. Soc.* **1977**, *124*, 1854. (c) Evans, A. G.; Evans, J. C.; Baker, M. W. *J. Am. Chem. Soc.* **1977**, *99*, 5882. (d) Bruinink, J.; Kregting, C. G. A. *J. Electrochem. Soc.* **1978**, *125*, 1397. (e) Furue, M.; Nozakura, S. *Chem. Lett.* **1980**, *9*, 821. (f) Harriman, A; West, M. A. *Photogeneration of Hydrogen*; Academic Press: London, 1982. (g) Grätzel, M. *Energy Resources through Photochemistry and Catalysis*; Academic Press: London, 1983. (h) Adar, E.; Degani, Y.; Goren, Z.; Willner, I. *J. Am. Chem. Soc.* **1986**, *108*, 4696. (i) Yasuda, A.; Mori, H.; Seto, J. *J. Appl. Electrochem.* **1987**, *17*, 567. (j) Claude-Montigny, B.; Merlin, A.; Tondre, C. *J. Phys. Chem.* **1992**, *96*, 4432. (k) Trabolsi, A.; Hmadeh, M.; Khashab, N. M.; Friedman, D. C.; Belowich, M. E.; Humbert, N.; Elhabiri, M.; Khatib, H. A.; Albrecht-Gary, A.-M.; Stoddart, J. F. *New J. Chem.* **2009**, *33*, 254.
(24) (a) Kosower, E. M.; Hajdu, J. *J. Am. Chem. Soc.* **1971**, *93*, 2534. (b) Gueder, W.; Hünig, S.; Suchy, A. *Tetrahedron* **1986**, *42*, 1665.
(25) Jeon, W. S.; Ziganshina, A. Y.; Lee, J. W.; Ko, Y. H.; Kang, J.-K.; Lee, C.; Kim, K. *Angew. Chem.* **2003**, *115*, 4231.
(26) (a) Trabolsi, A.; Khashab, N.; Fahrenbach, A. C.; Friedman, D. C.; Colvin, M. T.; Cotí, K. K.; Benítez, D.; Tkatchouk, E.; Olsen, J.-C.; Belowich, M. E.; Carmielli, R.; Khatib, H. A.; Goddard, W. A. III; Wasielewski, M. R.; Stoddart, J. F. *Nat. Chem.* **2010**, *2*, 42. (b) Li, H.; Fahrenbach, A. C.; Dey, S. K; Basu, S.; Trabolsi, A.; Zhu, Z.; Botros, Y. Y.; Stoddart, J. F. *Angew. Chem., Int. Ed.* **2010**, *49*, 8260. (c) Li, H.; Fahrenbach, A. C.; Coskun, A.; Zhu, Z.; Barin, G.; Zhao, Y.-L.; Botros, Y. Y.; Sauvage, J.-P.; Stoddart, J. F. *Angew. Chem., Int. Ed.* **2011**, *50*, 6782.
(27) Dichtel, W. R.; Miljanić, O. Š.; Zhang, W.; Spruell, J. M.; Patel, K.; Aprahamian, I.; Heath, J. R.; Stoddart, J. F. *Acc. Chem. Res.* **2008**, *41*, 1750.
(28) Takeshi, E.; Ageishi, K.; Okawara, M. *J. Org. Chem.* **1986**, *51*, 4309.
(29) In both cases, the crystals obtained were purple/black needles that were handeled under ambient conditions and in the presence of atmospheric oxygen. Crystal data for $[CBPQT^{2(\bullet+)}{\cdot}2PF_6^- \subset MV^{\bullet+}{\cdot}PF_6^-]$: $C_{36}H_{32}N_4{\cdot}C_{12}H_{14}N_2{\cdot}3(PF_6){\cdot}4(CH_3CN)$, $M_r$ = 1306.03, crystal size 0.10 × 0.09 × 0.09 mm$^3$, monoclinic, space group $P2_1/c$, $a$ = 9.702(7) Å, $b$ = 14.786(9) Å, $c$ = 21.131(2) Å, $\beta$ = 91.072(5)°, $V$ = 3031.2(5) Å$^3$, $Z$ = 2, $\rho_{calc}$ = 1.431, $T$ = 100(2) K, $R_1(F^2 > 2\sigma F^2)$ = 0.0469, $wR_2$ = 0.1313. Crystal data for $[CBPQT^{2(\bullet+)}{\cdot}2PF_6^-]$: $C_{36}H_{32}N_4{\cdot}2(PF_6)$, $M_r$ = 810.60, crystal size 0.30 × 0.10 × 0.10 mm$^3$, orthorhombic, space group *Pbam*, $a$ = 10.142(3) Å, $b$ = 21.863(0) Å, $c$ = 10.076(9) Å, $V$ = 2230.03(2) Å$^3$, $Z$ = 2, $\rho_{calc}$ = 1.207, $T$ = 100(2) K, $R_1(F^2 > 2\sigma F^2)$ = 0.1020, $wR_2$ = 0.3127.
(30) Data were collected at 100 K using a Bruker d8-APEX II CCD diffractometer (Cu K$\alpha$ radiation, $\lambda$ = 1.54178 Å). Intensity data were collected using $\omega$ and $\varphi$ scans spanning at least a hemisphere of reciprocal space for all structures (data were integrated using SAINT). Absorption effects were corrected on the basis of multiple equivalent reflections (SADABS). Structures were solved by direct methods (SHELXS) and refined by full-matrix least-squares against $F^2$ (SHELXL). Hydrogen atoms were assigned riding isotropic displacement parameters and constrained to idealized geometries. The crystal data for $[CBPQT^{2(\bullet+)}{\cdot}2PF_6^-]$ contained diffuse, disordered solvent molecules that suggested penetration through the macrocycle consistent with acetonitrile but could not be adequately modeled. The bypass procedure in Platon was used to remove the electronic contribution from these solvents. The total potential solvent accessible void volume was 319 Å$^3$, and the electron count per cell is 73. As the exact solvent content is not known, the reported formula reflects only the atoms used in the refinement.
(31) Hunter, C. A.; Sanders, J. K. M. *J. Am. Chem. Soc.* **1990**, *112*, 5525.
(32) Bockman, T. M.; Kochi, J. K. *J. Org. Chem.* **1990**, *55*, 4127.
(33) Benítez, D.; Tkatchouk, E.; Yoon, I.; Stoddart, J. F.; Goddard, W. A. *J. Am. Chem. Soc.* **2008**, *130*, 14928.
(34) Truhlar, D. G. *J. Am. Chem. Soc.* **2008**, *130*, 16824.
(35) Reed, A. E.; Weinstock, R. B.; Weinhold, F. *J. Chem. Phys.* **1985**, *83*, 735.

(36) Choi, J. W.; Flood, A. H.; Steuerman, D. W.; Nygaard, S.; Braunschweig, A. B.; Moonen, N. N. P.; Laursen, B. W.; Luo, Y.; Delonno, E.; Peters, A. J.; Jeppesen, J. O.; Xe, K.; Stoddart, J. F.; Heath, J. R. *Chem.—Eur. J.* **2006**, *12*, 261.
(37) Raymo, F. M.; Bartberger, M. D.; Houk, K. N.; Stoddart, J. F. *J. Am. Chem. Soc.* **2001**, *123*, 9264.
(38) This phenomenon of dimerization is indeed a common feature characterizing most types of radical cations including the viologen radicals ($K_{Dim}$ = 1.25 × $10^5$ $M^{-1}$ for $MV^{(\bullet+)}$·$MeSO_4$ in water) and is associated with significant spectroscopic changes, for example, the formation of new bands in the range of ∼550−570 nm as well as at approximately 900 nm. See: Monk, P. M. S.; Hodgkinson, N. M.; Ramzan, S. A. *Dyes Pigm.* **1999**, *43*, 207.
(39) By contrast with aqueous solutions, the monomer−dimer equilibrium is indeed usually not observed in polar organic solvents such as MeOH, MeCN, or DMF except at relatively high concentrations or low temperatures.
(40) EPR investigations, which were performed in MeCN on the $CBPQT^{2(\bullet+)}$ diradical dication, reveal a lack of hyperfine splitting in the spectrum, while the 1,1′-dibutynyl-4,4′-bipyrdinium $V^{\bullet+}$ radical cation displays the hyperfine splitting typically observed for these types of viologen derivatives. The lack of hyperfine splitting observed in the case of the $CBPQT^{2(\bullet+)}$ diradical dication is most likely a result of intramolecular dipole−dipole interactions between its two $BIPY^{\bullet+}$ radical cation units. For more details, see ref 26a.
(41) Although only the tail of this near-IR band has been observed because of the instrumental limitations (200−900 nm) of the absorption spectrophotometer employed during this investigation, we have reported previously using another spectrometer the spectrum of the $CBPQT^{2(\bullet+)}\subset V^{\bullet+}$ complex, which shows that this near-IR band has a maximum at 1075 nm. For more details, see ref 26a. In addition, there are conflicting rationalizations in the literature as to the nature of this near-IR absorption band typical of $BIPY^{\bullet+}$ radical dimers. We are of the belief that this near-IR band is a result of through-space intermolecular charge transfer similar to that observed for mixed-valent radical cation dimers. For further discussion, see: (a) Lü, J.-M.; Rosokha, S. V.; Kochi, J. K. *J. Am. Chem. Soc.* **2003**, *125*, 12161. (b) Sun, D.-L.; Rosokha, S. V.; Lindeman, S. V.; Kochi, J. K. *J. Am. Chem. Soc.* **2003**, *125*, 15950.
(42) Gampp, H.; Maeder, M.; Meyer, C. J.; Zuberbühler, A. D. *Talanta* **1985**, *32*, 95; **1985**, *32*, 251; **1986**, *33*, 943.
(43) Marquardt, D. W. *J. Soc. Ind. Appl. Math.* **1963**, *11*, 431.
(44) Maeder, M.; Zuberbühler, A. D. *Anal. Chem.* **1990**, *62*, 2220.
(45) Despite the inappropriate solvent conditions, that is, aqueous solutions favor pimerization processes, these thermodynamic data are comparable with those determined for pimerization of $MV^{\bullet+}$ as its methosulfate salt in $H_2O$ ($K_{Dim}$ = 1.25 × $10^5$ $M^{-1}$; log $K_{Dim}$ = 5.09). For further details, see the publications cited in ref 21.
(46) Hmadeh, M.; Fahrenbach, A. C.; Basu, S.; Trabolsi, A.; Benítez, D.; Li, H.; Albrecht-Gary, A. M.; Elhabiri, M.; Stoddart, J. F. *Chem.—Eur. J.* **2011**, *17*, 6076.
(47) Venturi, M.; Dumas, S.; Balzani, V.; Cao, J.; Stoddart, J. F. *New J. Chem.* **2004**, *28*, 1032.
(48) Hünig, S. *Pure Appl. Chem.* **1967**, *15*, 109.
(49) This scan rate of 30 V $s^{-1}$ is approaching the upper limit of our experimental capabilities, which is constrained by our use of a glassy carbon working electrode with a relatively large 0.071 $cm^2$ surface area.
(50) Share, A. I.; Parimal, K.; Flood, A. H. *J. Am. Chem. Soc.* **2010**, *132*, 1665.
(51) Gibb, B. C. *Nat. Chem.* **2009**, *1*, 252.
(52) Coskun, A.; Saha, S.; Aprahamian, I.; Stoddart, J. F. *Org. Lett.* **2008**, *10*, 3187.
(53) Smith, C. R. *Synlett* **2009**, 1522.
(54) Bio-Logic Company. *Biokine V3.0 User's Manuel*, Bio-Logic Company: Echirolles, France, 1991.
(55) Nelder, J. A.; Mead, R. *Comput. J.* **1965**, *7*, 308.
(56) Yeramian, E.; Claverie, P. *Nature* **1987**, *326*, 169.